

## Regular Article

Visual recognition of ortho-xylene based on its host-guest crystalline self-assembly with  $\alpha$ -cyclodextrin

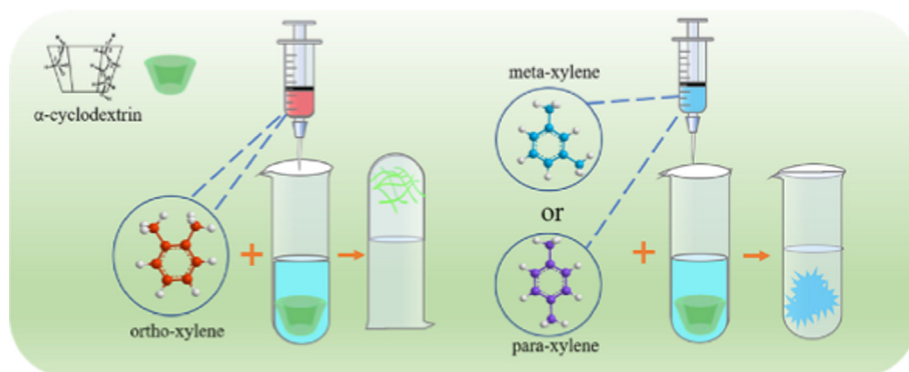
Weilin Qi<sup>a,1</sup>, Xuejiao Wang<sup>a,b,1</sup>, Zeyu Liu<sup>a</sup>, Kaerdun Liu<sup>a</sup>, Yifan Long<sup>c</sup>, Wanwan Zhi<sup>a</sup>, Cheng Ma<sup>a</sup>, Yun Yan<sup>a,\*</sup>, Jianbin Huang<sup>a,\*</sup>

<sup>a</sup> Beijing National Laboratory for Molecular Sciences (BNLMS), State Key Laboratory for Structural Chemistry of Unstable and Stable Species, College of Chemistry and Molecular Engineering, Peking University, Beijing 100871, PR China

<sup>b</sup> Fujian Provincial University Engineering Research Center of Industrial Biocatalysis, Fujian Normal University, Fuzhou 350007, PR China

<sup>c</sup> Department of Chemistry, University College London, London WC1E 6BT, UK

## GRAPHICAL ABSTRACT



## ARTICLE INFO

## Article history:

Received 21 January 2021

Revised 3 March 2021

Accepted 4 March 2021

Available online 15 March 2021

## Keywords:

Xylene isomers

$\alpha$ -Cyclodextrin

Supramolecular crystalline self-assembly

Macroscopic recognition

Hydrogel

## ABSTRACT

**Hypothesis:** Distinguishing substituted aromatic isomers is a challenging task because of the great similarity of their physicochemical properties. Considering xylene isomers have drastically different geometrical shapes, we predict this would show great impact on the self-assembling behavior of various xylene isomer@cyclodextrin inclusion complex.

**Experiments:** Through host-guest crystalline self-assembly, among three isomers, only *ortho*-xylene is capable to form hydrogels with  $\alpha$ -cyclodextrin. ROESY NMR, molecular simulations and circular dichroism spectra suggest that the ortho selectivity comes from the difference in the conformation of host-guest building block. The larger volume, and steric hinderance of the ortho isomer make it most possibly decrease their tendency to adopt more mobile orientations in cyclodextrin-based complex as meta and para isomers do, resulting in gel formation.

**Findings:** Herein, we report a novel, facile and environmentally-friendly protocol on the recognition of ortho benzene isomers using  $\alpha$ -cyclodextrin through host-guest crystalline self-assembly. Visual recognition of *ortho*-xylene is achieved through amplifying the structural difference of xylene isomers at molecular scale into macroscopic scale. We believe this work unveils subtle rules to control macroscopic

\* Corresponding authors at: College of Chemistry and Molecular Engineering, Peking University, Beijing 100871, PR China.

E-mail addresses: [yunyan@pku.edu.cn](mailto:yunyan@pku.edu.cn) (Y. Yan), [jbhuang@pku.edu.cn](mailto:jbhuang@pku.edu.cn) (J. Huang).

<sup>1</sup> Weilin Qi and Xuejiao Wang contributed equally to this work.

assemblies at the molecular level and highlights the potential of using macrocyclic compounds to improve the quality and reduce the energy bill for separation in petrochemical industry.

© 2021 Published by Elsevier Inc.

## 1. Introduction

With the ever-growing needs for chemical products geared by the fast development of industries, for instance, petrochemical engineering and medical industries, innovative strategies and materials are becoming significantly important to improve the efficiency, safety and energy bill of the relating chemical processes, especially those involved with isomers. For instance, xylenes are important industrial feedstocks for plastics, rubber, fibers, solvents, and fuels [1–4]. Ortho-xylene isomers, in particular, are vital chemicals that are used in large-scale polymers and solvents (o-dichlorobenzene and o-chlorotoluene) production [5]. However, the recognition and separation of o-xylene isomers from other xylene isomers has always been one of the most difficult problems due to their identical molecular weights and similar physical properties [6,7]. At present, several methods are effective for the recognition of xylene isomers, such as UV spectrometry, gas chromatography (GC), and low-pressure gas chromatography–ion trap mass spectrometry (LP-GC–IT-MS), which require costly and complex instrumentation [8–13]. Consequently, a variety of other sensors, such as metal organic frameworks (MOFs), conductive polymer-based sensors, and other materials, were endeavored [14–19]. So far, it still remains challenging to develop an easy and low-cost method for identification of xylene isomers at macroscopic scale [20].

On account of the similarities in the physical properties of these significant chemical raw materials [21], the geometry of these molecules is one of their most prominent distinguishing characteristics, hence materials capable of recognizing their geometry should prove to be promising in their recognition. Cyclodextrins (CyDs) are cyclic oligosaccharides possessing molecular-compatible cavities [22]. The exterior of the cavity is highly hydrophilic due to the presence of hydroxyl groups, while the interior is hydrophobic endowed by methylene groups. Besides, CyDs have a truncated cone structure since the diameter of the cavity on the rim with the primary hydroxyl groups is smaller than that on the rim with the secondary hydroxyl groups. This highly asymmetric geometry, the number of the constituting saccharides ( $\alpha$ ,  $\beta$ ,  $\gamma$ ), together with the strong hydrophobic nature of the cavity make CyDs suitable and fascinating hosts to selectively recognize and bind hydrophobic guests of various sizes [23–29], and has long been utilized in molecular recognition.

In the past decade, studies in our group reveal that the host-guest inclusion complex formed with CyDs and surfactants or other organic molecules with alkyl chains, including alkanes, alcohols, and amines, are all able to form crystalline self-assembly, such as vesicles, microtubes, fibers, lamellae, helical ribbons or even rhombics driven by hydrogen bonding between CyDs [30–36]. It is interesting to find that the self-assembled structure and the induced chirality in the CyD inclusion systems could be chain-length dependent, indicating the self-assembly can be significantly impacted by the subtle structural difference of the guest molecules [37]. Considering xylene isomers have drastically different geometrical shapes, we anticipate that this would show great impact on the self-assembling behavior of various xylene isomer/CyD inclusion complex.

In summary, our research puts forward a novel and facile host-guest crystalline protocol on visual recognition of *ortho*-xylene. In this work, we report that when o, m, p xylene isomers were used to

construct inclusion complex with  $\alpha$ -CyD in aqueous media, only o-xylene/ $\alpha$ -CyD complexes could form hydrogels, whereas the  $\alpha$ -CyD inclusion complexes with p- and m-isomers both separated into two phases in water. Microstructure observation revealed that ultralong nanofibers were formed in the o-xylene/ $\alpha$ -CyD system. In contrast, microribbons and blocks are formed in the m-xylene/ $\alpha$ -CyD and p-xylene/ $\alpha$ -CyD systems, respectively. In this way, we have amplified the structural difference of xylene isomers at molecular scale into macroscopic scale through host-guest crystalline self-assembly. We hope this research smooths the way for an in-depth study on the recognition properties of macrocyclic compounds in molecular self-assembly, which may shed lights for the macroscopic separation of xylene isomers in the future.

## 2. Experimental section

### 2.1. Materials

Ortho-xylene (OX, AR), *meta*-xylene (MX, AR), *para*-xylene (PX, AR) were purchased from Aladdin.  $\alpha$ -cyclodextrin ( $\alpha$ -CyD, AR), 2-ethyltoluene, 3-ethyltoluene 4-ethyltoluene, were purchased from Macklin. Distilled water was purified through Milli-Q Advantage A10 Ultrapure Water System. D<sub>2</sub>O (99.9%) and DMSO *d*<sub>6</sub> (99.9%) were purchased from Aldrich.

### 2.2. Sample preparation

The desired amounts of organic samples were added into the  $\alpha$ -CyD solutions and then the samples were vortex sufficiently (about 10 min) at room temperature. The resultant mixtures were thermostatically incubated at 25 °C (for at least 24 h) to obtain a white inverted immobile gel or precipitates. Gel and precipitates were collected by removal of the supernatants and lyophilized for further characterization.

### 2.3. Scanning electron microscope (SEM)

SEM measurements were performed using a Hitachi S4800 microscope at an acceleration voltage of 1 kV. A drop of the suspension was placed on clean silicon sheets and then dried in the vacuum drying oven (25 °C).

### 2.4. Nuclear magnetic resonance (NMR) studies

<sup>1</sup>H NMR and ROESY spectra experiments were performed on a Bruker ARX 500 MHz spectrometer at room temperature (25 ± 2 °C), using 5 mm standard NMR tubes. Deuterioxide (99.9%) was used to dissolve the precipitates for <sup>1</sup>H NMR spectra, all proton signals were calibrated with D<sub>2</sub>O signal at 4.800 ppm.; D<sub>2</sub>O (99.9%) was used to solve it for 2D-ROESY.

### 2.5. Circular dichroism (CD) measurements

Circular dichroism (CD) spectra were obtained on a JASCO J-810 spectrometer and used to investigate the ICD of the sample suspension. The light path length of the quartz cell used is 0.1 mm. Scanning speed was set at 100 nm/min. Data was collected at a response of 2 sec and accumulated twice.

## 2.6. Theoretical simulations

An extensive dynamic and structural characterization of the system was provided to support our model. We used the Visualizer module in Materials Studio to build a structural model of small aromatic molecules. At the same time, based on the crystal data of  $\alpha$ -cyclodextrin, a structural model of  $\alpha$ -cyclodextrin was constructed in the Visualizer module. We used the Construction function of the Amorphous cell module to construct a molecule containing an  $\alpha$ -cyclodextrin and a Periodic amorphous unit of small aromatic molecules. All kinetic calculations were based on a PCFF force field and cutoff was on account of non-bond interaction. We used the Minimizer function in the Discover module of Material Studio to minimize the potential energy of several possible conformations of the inclusions formed by  $\alpha$ -cyclodextrin and aromatic molecules and find the lowest potential energy in the inclusions of the host and guest Conformation.

The separation and spline width were 8.5 Å and 0.0 Å, respectively and the buffer width was set at 0.5 Å. The constructed periodic unit was applied and the Smart Minimizer method was used to minimize potential energy. We performed 10 ps of NVT ensemble molecular dynamics. The simulation temperature selection was set at 298 K and time step was set at 1 fs, while full trajectory information was recorded every 1000 steps. Structures of  $\alpha$ -cyclodextrin and aromatic inclusion complexes can be obtained in 10 simulations.

Besides, solvent is not considered in our simulation. First, the interior of cyclodextrin's cavity is highly hydrophobic endowed by methylene groups and none of water molecule was found to move into the cavity in the presence of the guest [38]. Secondly, the main focus of our simulation is to probe the energetics difference raised by steric hinderance, which is not affected by solvent.

## 2.7. Small-angle X-ray scattering instrument (SAXS) measurements

The lyophilized gel and precipitate sample were measured on a high-flux SAXS (Anton Parr) equipped with a Kratky block collimation system.

## 2.8. Fourier transform infrared (FT-IR) absorption

FT-IR measurements were performed on Nicolet Magna IR 750 equipped with an infrared microspectrography (Thermo Scientific Co., USA).

## 2.9. Rheology

Rheological properties were measured by a Thermo Haake RS300 rheometer with cone and plate geometry (35 mm diameter, 0.105 mm cone gap). The temperature was kept at 25 °C and a water trap was used to minimize water evaporation from the sample. Frequency spectra were conducted in the linear viscoelastic regime of the samples determined from dynamic strain sweep measurements.

## 2.10. Fourier transform ion cyclotron resonance mass spectrometer (FT-MS)

Mass spectra were recorded on a Bruker Apex IV FTMS operating in a ESI positive mode.

## 3. Results and discussion

### 3.1. Macroscopic recognition and microstructures of xylene isomers@ $\alpha$ -CyD systems

Xylene isomers were used to build host–guest systems with  $\alpha$ -cyclodextrin. We chose  $\alpha$ -cyclodextrin rather than  $\beta$ -cyclodextrin or  $\gamma$ -cyclodextrin for better size matching with xylene isomers, because  $\beta$ -cyclodextrin or  $\gamma$ -cyclodextrin has larger cavity than all the three xylene isomers which shows no distinct difference in the ability of complexing with the three isomers. The binding constant of OX, MX, PX with  $\alpha$ -CyD is 22 M<sup>-1</sup>, 40 M<sup>-1</sup>, 72 M<sup>-1</sup>, respectively and  $\Delta G_{\text{complex}}$  of OX, MX, PX with  $\alpha$ -CyD is -8 kJ/mol, -9 kJ/mol, -11 kJ/mol [39]. Fig. 1 shows the geometry information of  $\alpha$ -CyD and the xylene isomers employed in this study.

The inclusion complexes were obtained by adding different xylene isomers respectively into the transparent solution of  $\alpha$ -cyclodextrin and then vortex about 10 min. White precipitates were obtained in MX@ $\alpha$ -CyD and PX@ $\alpha$ -CyD systems. Surprisingly, hydrogels capable of supporting their own weight in inverted tubes were formed in the OX@ $\alpha$ -CyD system. In all the tested hydrogels, the rheological data showed that the storage modulus ( $G'$ ) is 3–4 times greater than the loss modulus ( $G''$ ), indicating that they are elastic rather than viscous materials, which is a distinguishing feature of gel materials (Fig. S1).

SEM images demonstrate that the microstructures in the OX@ $\alpha$ -CyD hydrogel are ultralong nanofibers. These fibers are flexible, and their diameter is about 150 nm, whereas their length is in the order of tens of millimeters. In contrast, the MX@ $\alpha$ -CyD and PX@ $\alpha$ -CyD precipitates are composed of much shorter and wider structures. Microrods with their widths and lengths around 1 and 20  $\mu\text{m}$ , respectively, were formed in the MX@ $\alpha$ -CyD system, while bulk planar flakes were formed in the PX@ $\alpha$ -CyD. It is noticed that the ultralong nanofibers in the OX@ $\alpha$ -CyD system have entangled into dense networks, which explains why the OX@ $\alpha$ -CyD system can sustain stress which accounts for gel formation.

### 3.2. Conformation of the building block in xylene isomers@ $\alpha$ -CyD systems

#### 3.2.1. NMR(ROESY) analysis to probe the inclusion mode

NMR and FT-MS measurements demonstrate the formation of the 1:1 inclusion complex in all three systems (Figs. S2, S3). To investigate why the three xylene isomers have caused such large differences both at micro and macro scales, ROESY (Rotating-Frame Overhauser Effect Spectroscopy) NMR measurements were conducted to examine the conformation of different xylene isomers in the cavity of  $\alpha$ -CyD. Traditional NOESY (Nuclear Trans-limit Effect Spectroscopy) method is limited in the mass range of 1000~2000 Da due to the unsatisfactory tumbling rates of the molecules. Therefore, spin-lock techniques such as Rotating Frame Overhauser effect spectroscopy (ROESY) are ideal methods to study the spatial interactions in CyD complexes. In all instances, COSY (Correlated Spectroscopy) experiments were also employed to definitively identify the intermolecular components and rule out the intermolecular interactions. If protons in the guest molecule are close enough to the  $\alpha$ -CyD hydrogen (about 4 Å), spatial interaction will occur and a cross peak will be observed in ROESY (the number of circles represent the interaction intensity), so ROESY can be applied to determine the position of the guest in the CyD cavities [40–42].

The assignment of NMR spectra is according to literature (Fig. S5) [43]. Fig. 2a shows the schematic structure of  $\alpha$ -CyD with

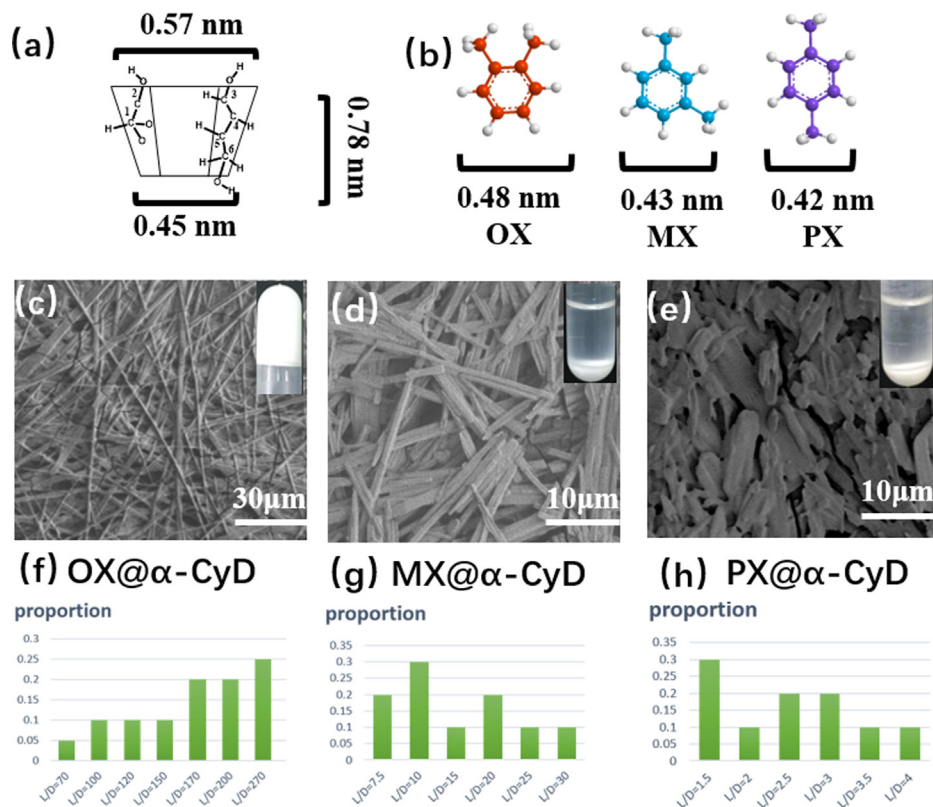


**Fig. 1.** Schematic structures and molecular dimensions of (a)  $\alpha$ -cyclodextrin and (b) xylene isomers employed in this study. Photographs, SEM images, length-diameter ratio statistics of xylene isomer@ $\alpha$ -CyD systems: (c,f) OX@ $\alpha$ -CyD hydrogel, (d,g) MX@ $\alpha$ -CyD precipitate, (e,h) PX@ $\alpha$ -CyD precipitate. (70:70 mM) systems.

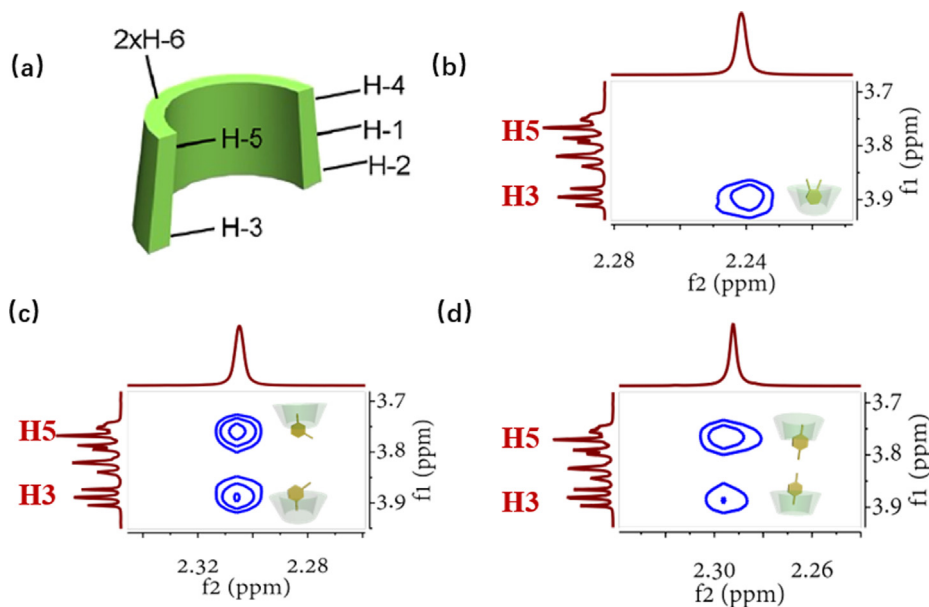


**Fig. 2.** (a) Schematic illustration of the structure of  $\alpha$ -CyD [44]; 2D-NMR (ROESY) spectrum and the schematic illustration (insets) of building block of (b) OX@ $\alpha$ -CyD, (c) MX@ $\alpha$ -CyD, (d) PX@ $\alpha$ -CyD (1:1) in  $D_2O$ .

numbered protons. The H-3, H-5, and one of the H-6 protons are inside of the  $\alpha$ -CyD cavity and H-3 and H-5 are around the wider rim while H-5 are near the narrower rim. By analyzing the correlations between xylene protons and H-3/ H-5, one can envisage the orientation of the guest within the  $\alpha$ -CyD cavity.

Fig. 2b reveals that only one correlation occurs between OX and  $\alpha$ -CyD, ascribing the methyl protons of OX ( $\delta$ 2.24 ppm) and H3 of  $\alpha$ -CyD. In consideration of that H3 is located around the wider rim

of  $\alpha$ -CyD, the only correlation peak shows that the methyl group of OX is positioned predominantly at the wider rim of  $\alpha$ -CyD. In contrast, the methyl protons of MX/PX form correlations with both the H3 and H5 protons of  $\alpha$ -CyD. These results unambiguously suggest that OX is able to thread into the cavity of  $\alpha$ -CyD with a preferred orientation, whereas MX/PX is unable to do this (Fig. 2c and Fig. 2d).

We speculate that the specific orientation of OX in the cavity of  $\alpha$ -CyD is probably related with its molecular size. Chem 3D model-

ing (Fig. 1b) suggests that width of the OX molecule (distance between the two methyl groups) is about 4.8 Å, which is larger than the diameter of the narrower rim (4.5 Å) of  $\alpha$ -CyD but smaller than its diameter of the wider rim (5.7 Å). Therefore, OX would thread into the cavity of  $\alpha$ -CyD from the wider rim. In contrast, the widths of MX and PX are both around 4.2 Å, which is smaller even than the size of the narrower rim of  $\alpha$ -CyD. This means that MX and PX are able to thread into the cavity of  $\alpha$ -CyD from both the narrower and wider rim. Obviously, this threading at molecular scale have triggered the drastic difference at micro and macro scale.

### 3.2.2. Computational studies on orientation of xylene isomers in the cavity of $\alpha$ -CyD

In order to understand the preferred conformation of building block, theoretical computations based on molecular dynamics (MD) were carried out to gain a better insight into the interaction energetics of xylene with  $\alpha$ -CyD. The potential energy of corresponding conformation is summarized in Fig. 3a.

We considered 6 conformations (shown in Fig. 3) according to 2D NMR experiments. There is only correlation between methyl protons of OX and cyclodextrin's wider rims, thus we can expect the dominating conformation of OX@ $\alpha$ -CyD is Fig. 3b with methyl towards the wider rim. Chem 3D modeling (Fig. 1b) suggests that width of the OX molecule (distance between the two methyl groups) is about 4.8 Å, which is larger than the diameter of the narrower rim (4.5 Å) of  $\alpha$ -CyD, so we chose conformation in Fig. 3c to show its energy disadvantage due to steric hinderance. 2D NMR indicates there is equivalent correlation between methyl protons of MX and both rims of cyclodextrin and the widths of MX and PX are both around 4.2 Å, which is smaller even than the size of the narrower rim (4.5 Å) of  $\alpha$ -CyD. Therefore, similar to OX@ $\alpha$ -CyD, we also chose two conformations accommodated at the wider and narrower rim respectively for MX@ $\alpha$ -CyD and PX@ $\alpha$ -CyD to show there is no steric hinderance. Other conformations could be excluded by 2D NMR and molecular size fitting analysis (Fig. S6).

When the two methyl groups are accommodated at the wider rims of  $\alpha$ -CyD (Fig. 3b), the structure-optimized potential energy of the OX@ $\alpha$ -CyD system is 83.69 kcal/mol. However, when the two methyl groups are positioned at the narrower rims of the cyclodextrin (Fig. 3c), the potential energy of the system after structural optimization is 101.90 kcal/mol, which is almost 20 kcal/mol higher than the former. It can be concluded that the former conformation is more stable, which is the predominant conformation because of the large steric hinderance when the methyl groups were placed at the narrower rims.

However, MD simulation results suggest that in the case of MX and PX, the energies for the inclusion complexes threaded from both rims are rather close, which is 70.36 and 74.40 kcal/mol, respectively, for the MX@ $\alpha$ -CyD system (Fig. 3d and e), and 67.94 and 68.58 kcal/mol for the PX@ $\alpha$ -CyD system (Fig. 3f and g). Obviously, there is no steric hinderance for both conformations which explains why *meta*-xylene has no preferred orientation when projecting into the cavity of  $\alpha$ -CyD.

### 3.2.3. Induced circular dichroism studies

Chiral (non-racemic) compounds can induce circular dichroism (ICD) signals in the ultraviolet or visible region of non-chiral compounds through intermolecular interactions. Cyclodextrin's cavity is known to be chiral and it can transfer chirality to guests that are not optically active through host-guest interactions [45]. According to report, the sign of the induced circular dichroism (CD) signals depends on the guest's orientation in CyDs. If a guest locates inside the cavity and its dipole transition moment is polarized parallel to the axis of CyD, the sign of CD is positive, otherwise the sign is negative in situation of above (outside) the cavity

[40,46,47]. However, this only occurs when the guest thread into the cavity of CyD with a preferred orientation. On the contrary, if the threading direction of the guest to the cavity of CyDs is not selective, no CD can be observed. It remains challenging to control the threading direction of the guest in cyclodextrin assembly, and the coexistence of two orientations will result in a mixture that lose chirality, which is racemic. For this reason, the ICD spectra are indicative of the actual conformation of the host-guest inclusion complex.

The induced circular dichroism (CD) of the supramolecular system of the xylene@ $\alpha$ -CyD is examined. A positive CD signal is obtained at 206 nm for the OX@ $\alpha$ -CyD system corresponding to its absorption spectrum of xylene, while the MX@ $\alpha$ -CyD and PX@ $\alpha$ -CyD system are CD silent (Fig. 4a). This is in perfect agreement with the 2D NMR measurements and molecular dynamic simulations that OX predominantly threads into the cavity of  $\alpha$ -CyD from the wider rim. Furthermore, the positive ICD signal accounts for the fact that the guest's electronic dipole transition moment is exactly inside the cavity of  $\alpha$ -CyD, which is in line with the prediction of Harata-Kodaka's rule (Fig. 4b, c, d).

## 3.3. Host-guest assembly process of xylene isomers@ $\alpha$ -CyD systems

### 3.3.1. Role of hydrogen bonding in the self-assembly structures

The abundant hydroxyl groups of  $\alpha$ -Cyds offer multiple H-bond sites, which is a natural driving force to realize host-guest assembly [48,49]. The subsequent urea addition experiments confirmed this. Urea is a common H-bond breaker, which can be added to break hydrogen bonding in corresponding system. As urea was added into the gel or precipitation in the present study, disassembly of the microstructures was observed. Take OX@ $\alpha$ -CyD gel as an example (Fig. 5). The hydrogel turned into transparent sol when 5 M urea was added (Fig. 5a), indicating that the H-bonds were the main driving force for hydrogel formation. Moreover, we conducted a FT-IR experiment to further verify the presence of hydrogen bonding in the systems. The hydroxyl band for the pure lyophilized powder of  $\alpha$ -CyD appears at 3365  $\text{cm}^{-1}$  (Fig. 5b), while that for the lyophilized o-xylene@ $\alpha$ -CyD gel, m-xylene@ $\alpha$ -CyD precipitation and p-xylene@ $\alpha$ -CyD precipitation shifted to a lower wavenumber of 3359, 3353 and 3357  $\text{cm}^{-1}$ , respectively, demonstrating the formation of hydrogen bonds in three xylene isomers@ $\alpha$ -CyD systems [50,51].

### 3.3.2. d-spacing of the assembly structures

To adequately explore the microscale structure difference caused by xylene isomers, we have conducted the small-angle X-ray scattering (SAXS) of xylene isomers@ $\alpha$ -CyD complexes (Fig. 5c). All the three systems show characteristic diffractions at  $q = 0.82$  and  $1.24 \text{ \AA}^{-1}$ , which indicates a channel-type arrangement of  $\alpha$ -CyD (Fig. 5d). At the same time, the SAXS profiles for all the three systems show Bragg peaks with regular spacing, which is a characteristic pattern for typical lamellar structures [34,52–54]. By applying the first peak's position (the first harmonic  $q_1$ ) to the equation  $d = 2\pi/q_1$ , we can acquire the repeated distance  $d$  (around 1.5 nm) of the lamellar structures. Accounting that the height of one  $\alpha$ -CyD is 0.78 nm, the  $d$ -spacing of 1.5 nm corresponds to a building block of 2xylene@2 $\alpha$ -CyD. However, the  $d$ -spacing of OX@ $\alpha$ -CyD gel system (1.58 nm) is larger than MX@ $\alpha$ -CyD or PX@ $\alpha$ -CyD systems (1.52 nm). This is up to our expectation, since the OX molecule would outcrop a little in the wider rim, whereas MX and PX were completely buried in the cavity of  $\alpha$ -CyD due to their different 'width'.

This may also explain the difference in the self-assembled structure of OX@ $\alpha$ -CyD from its counterparts. The outcropping of

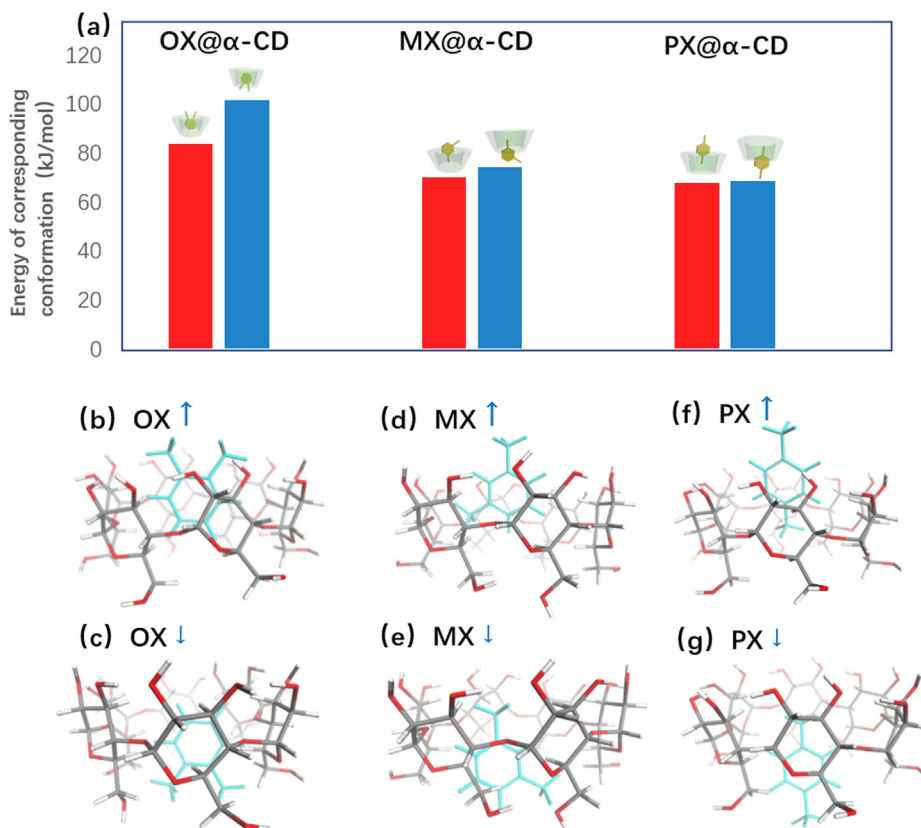


**Fig. 3.** (a) Column plot of the energies for the three pair of conformations. Snap shows of molecular simulation optimized structures of xylene isomers with α-CyD, OX@α-CyD complex with two methyl groups (b) predominantly oriented toward the wider rim of α-CyD, (c) oriented toward the narrower rim of α-CyD; MX@α-CyD complexes with (d) MX predominantly oriented toward the wider rim of α-CyD, (e) MX oriented toward the narrower rim of α-CyD; PX@α-CyD complexes with (f) PX predominantly oriented toward the wider rim of α-CyD, (g) PX oriented toward the narrower rim of α-CyD. The xylene isomers were colored blue for the sake of clarity. (For interpretation of the references to colour in this figure legend, the reader is referred to the web version of this article.)

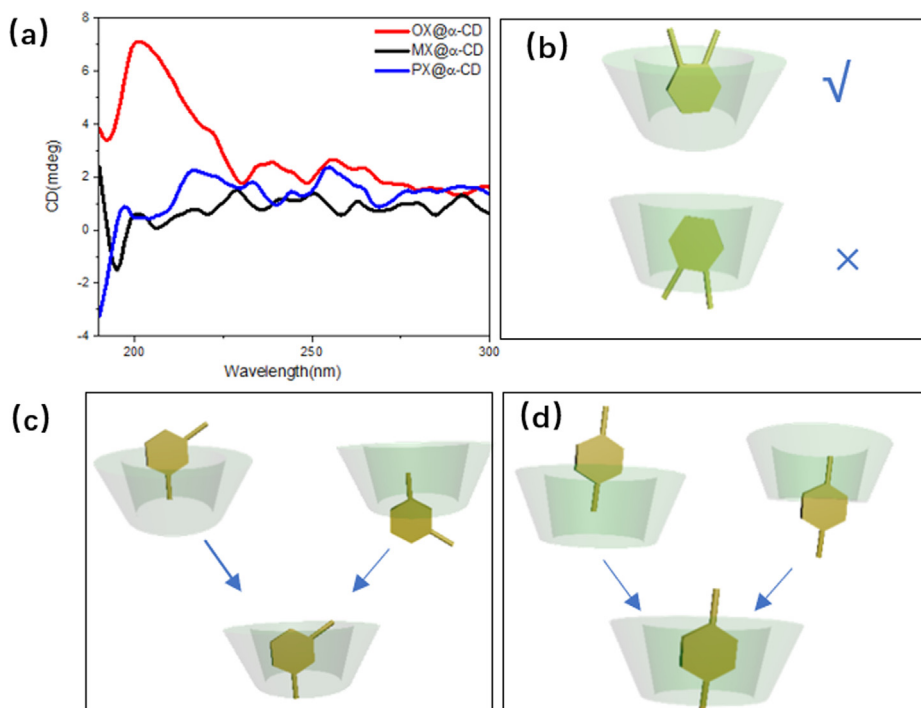


**Fig. 4.** (a) Circular dichroism spectroscopy (CD Spectrum) of xylene isomers@α-CyD (75:75 mM) systems, Schematic representations of different inclusion modes of xylene isomers@α-CyD complexes: (b) o-xylene@α-CyD, the upper is the predominant orientation, (c) m-xylene@α-CyD, m-xylene threads into the cyclodextrin cavity through both rims, (d) p-xylene@α-CyD, p-xylene threads into the cyclodextrin cavity through both rims.

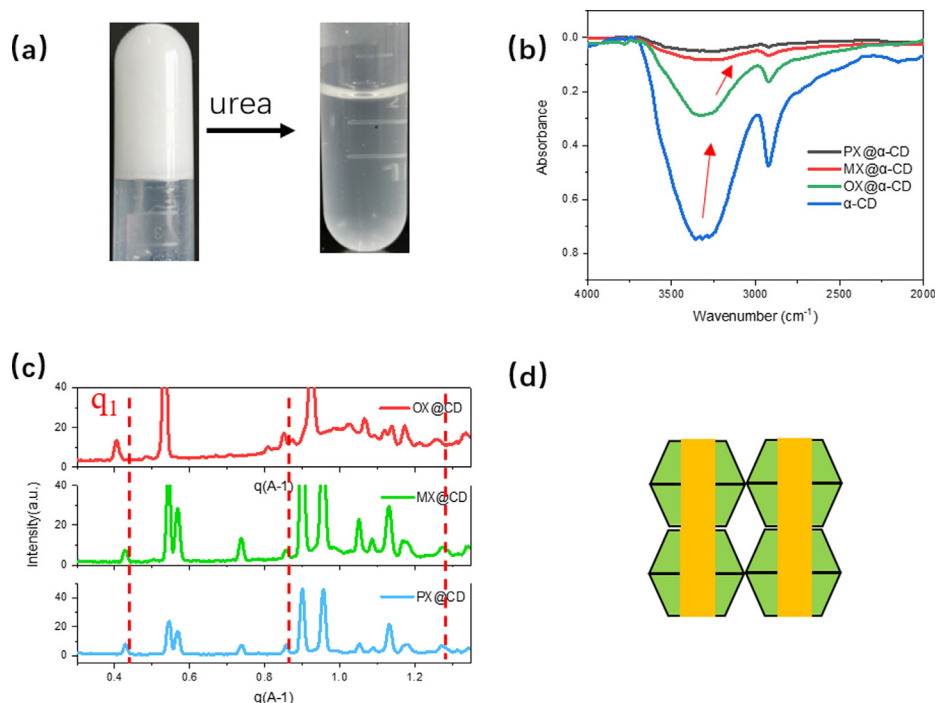


**Fig. 5.** (a) Visual appearance images of gel-sol transition caused by adding 5 M urea at 25 °C, (b) FT-IR spectra of  $\alpha$ -CyD powder, the lyophilized xylene isomers@ $\alpha$ -CyD assemblies, (c) SAXS profile of lyophilized xylene isomers@ $\alpha$ -CyD (75:75 mM) assemblies, (d) Schematic representations of channel type arrays in xylene isomers@ $\alpha$ -CyD complexes.

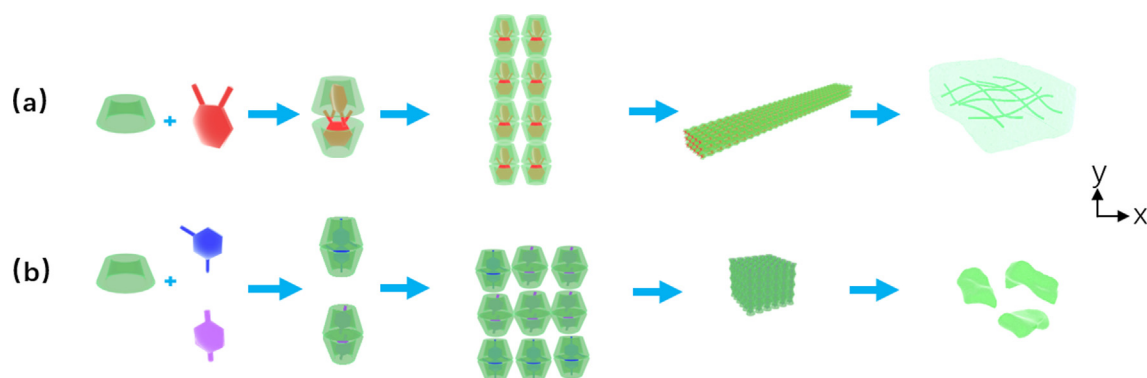


**Fig. 6.** Schematic diagram of possible self-assembly route in the xylene isomers@ $\alpha$ -CyD complexes: a) o-xylene@ $\alpha$ -CyD, b) m-xylene@ $\alpha$ -CyD, and p-xylene@ $\alpha$ -CyD.

the methyl groups of OX on the wider rim of  $\alpha$ -CyD makes it disadvantageous for the hydrogen bonding between the  $\alpha$ -CyDs vertical to its axis (X direction), so that the channel type arrangement (Y direction) are more prominent than that in the other two systems. As a result, ultralong nanofibers were formed, and gelation occurs. In contrast, the hydrogen bonding along X direction in the MX and PX@ $\alpha$ -CyD systems are easier than that in the OX@ $\alpha$ -CyD system, so that the selective growth along the channel direction is retarded, as illustrated in Fig. 6.

### 3.4. Recognition of other disubstituted benzene isomers

To confirm our speculation on *ortho*-selection assembly, we extended our research to ethyltoluene system (Fig. 7), and the regioselective recognition was also achieved. The 3-ethyl toluene@ $\alpha$ -CyD and 4-ethyl toluene@ $\alpha$ -CyD systems were white precipitates, while a stable gel can be obtained when 2-ethyl toluene was utilized under the same condition. The selective dis-

crimination of the isomers has been further confirmed by SEM, circular dichroism spectra.

The ethyl toluene@ $\alpha$ -CyD systems exhibited consistent assembly behaviors as the xylene system. After ICD testing, a similar result is obtained again (Fig. 7e): a positive CD signal is obtained at wavelength matched with the UV absorption of 2-ethyl toluene. Meanwhile, 3-ethyl toluene@ $\alpha$ -cyclodextrin precipitation system and the 4-ethyl toluene@ $\alpha$ -cyclodextrin precipitation system are CD silent, which could be explained through a mechanism analogous to xylene@ $\alpha$ -CyD systems.

## 4. Conclusion

In summary, we provide a facile and environmentally friendly strategy on the visual recognition of *ortho* benzene isomers using  $\alpha$ -cyclodextrin through host-guest crystalline self-assembly. Among three isomers, only o-xylene is capable to form hydrogels with  $\alpha$ -cyclodextrin, whereas the  $\alpha$ -CyD inclusion complexes with

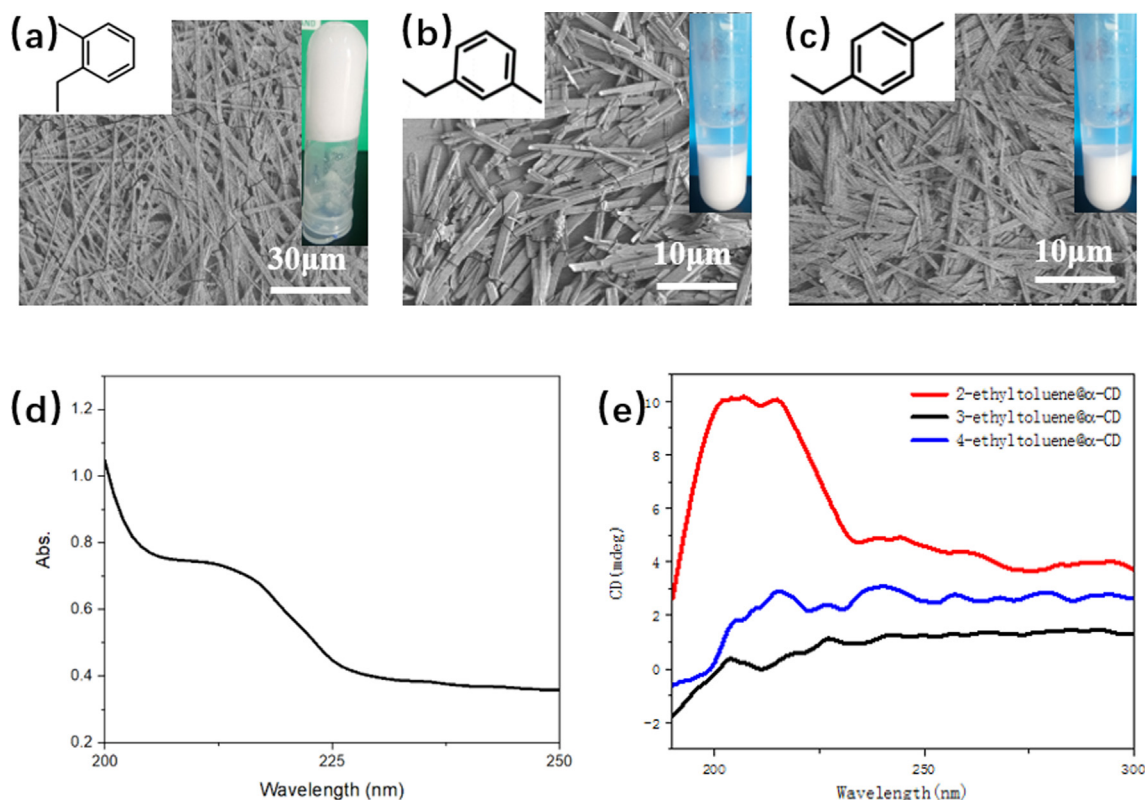


**Fig. 7.** Photographs and SEM images of ethyl toluene isomer@ $\alpha$ -CyD systems: (a) 2-ethyl toluene@ $\alpha$ -CyD hydrogel; (b) 3-ethyl toluene@ $\alpha$ -CyD precipitate; (c) 4-ethyl toluene@ $\alpha$ -CyD precipitate (50:50 mM) systems; (d) Absorption Spectrum and (e) Circular dichroism spectroscopy (CD Spectrum) of ethyltoluene isomers@ $\alpha$ -CyD (20:20 mM) systems.

*p*- and *m*-isomers both separated into two phases in water. As such *o*-xylene is recognized over other derivatives, 2D NMR, molecular dynamics and ICD spectrometry indicate that the asymmetry of the wider and narrower rims of the cyclodextrin endows it high shape selectivity to control the orientation of the guest in the cavity of CD. Unlike *m*-xylene and *p*-xylene, the methyl groups of *o*-xylene locate predominantly at the wider rim of  $\alpha$ -CyD and thus different conformation of building block results in distinctive assembly behavior of the isomers.

Compared to previous researches on xylene recognition (Table S1), our manuscript puts forward a novel and facile crystalline self-assembly protocol on this issue. Generally, recognition of xylene isomers requires costly and complex instrumentation [8–9,13] or tedious synthesis of sensors [14,18,55–56]. Cyclodextrins are green, economic and versatile host in assembly, which show great potential in recognition and separation [23–25,27–29]. Through cyclodextrin-based host–guest crystalline assembly, we have amplified the structural difference of xylene isomers at molecular scale into macroscopic scale and achieved the visual recognition of *ortho*-xylene in a facile and environmentally friendly way. This work highlights the role of molecular recognition research employing macrocyclic compounds to improve the quality and energy bill of critical industrial separations by host–guest crystalline self-assembly. We expect that crystalline self-assembly, as a bottom-up strategy, displays great potential in benzene series recognition and separation in the future. In this way, we believe our design is novel and versatile and our work advances and broadens the development of colloid and interface chemistry.

#### CRediT authorship contribution statement

**Weilin Qi:** Methodology, Formal analysis, Investigation, Resources, Data curation, Visualization, Writing - original draft.

**Xuejiao Wang:** Conceptualization, Methodology, Formal analysis, Resources. **Zeyu Liu:** Methodology. **Kaerdun Liu:** Methodology. **Yifan Long:** Methodology. **Wanwan Zhi:** Methodology. **Cheng Ma:** Methodology. **Yun Yan:** Writing - review & editing, Supervision, Funding acquisition. **Jianbin Huang:** Writing - review & editing, Supervision, Funding acquisition.

#### Declaration of Competing Interest

The authors declare that they have no known competing financial interests or personal relationships that could have appeared to influence the work reported in this paper.

#### Acknowledgments

This work is supported by National Natural Science Foundation of China (21633002, 91856120, 21972003).

#### Appendix A. Supplementary material

Supplementary data to this article can be found online at <https://doi.org/10.1016/j.jcis.2021.03.024>.

#### References

- [1] C. Seechurn, M.O. Kitching, T.J. Colacot, V. Snieckus, Palladium-catalyzed cross-coupling: A historical contextual perspective to the 2010 Nobel Prize, *Angew. Chem.-Int. Edit.* 51 (21) (2012) 5062–5085.
- [2] D.S. Sholl, R.P. Lively, Seven chemical separations to change the world, *Nature* 532 (7600) (2016) 435–437.
- [3] Y. Yang, P. Bai, X. Guo, Separation of xylene isomers: A review of recent advances in materials, *Ind. Eng. Chem. Res.* 56 (50) (2017) 14725–14753.
- [4] M. Lusi, L.J. Barbour, Solid-vapor sorption of xylenes: prioritized selectivity as a means of separating all three isomers using a single substrate, *Angew. Chem.-Int. Edit.* 51 (16) (2012) 3928–3931.

- [5] G. Zhang, A.-H. Emwas, U.F.S. Hameed, S.T. Arold, P. Yang, A. Chen, J.-F. Xiang, N.M. Khashab, Shape-induced selective separation of ortho-substituted benzene isomers enabled by cucurbit 7 uril host macrocycles, *Chem* 6 (5) (2020) 1082–1096.
- [6] A. Torres-Knoop, R. Krishna, D. Dubbeldam, Separating xylene isomers by commensurate stacking of p-xylene within channels of MAF-X8, *Angew. Chem.-Int. Edit.* 53 (30) (2014) 7774–7778.
- [7] M. Minceva, A.E. Rodrigues, Modeling and simulation of a simulated moving bed for the separation of p-xylene, *Ind. Eng. Chem. Res.* 41 (14) (2002) 3454–3461.
- [8] Z.-Y. Gu, X.-P. Yan, Metal-organic framework MIL-101 for high-resolution gas-chromatographic separation of xylene isomers and ethylbenzene, *Angew. Chem.-Int. Edit.* 49 (8) (2010) 1477–1480.
- [9] J.M. Dela Cruz, V.V. Lozovoy, M. Dantus, Isomeric identification by laser control mass spectrometry, *J. Mass Spectrom.* 42 (2) (2007) 178–186.
- [10] P.E. Joos, A.F.L. Godoi, R. De Jong, J. de Zeeuw, R. Van Grieken, Trace analysis of benzene, toluene, ethylbenzene and xylene isomers in environmental samples by low-pressure gas chromatography - ion trap mass spectrometry, *J. Chromatogr. A* 985 (1–2) (2003) 191–196.
- [11] F. Vogt, M. Tacke, M. Jakusch, B. Mizaiakoff, A UV spectroscopic method for monitoring aromatic hydrocarbons dissolved in water, *Anal. Chim. Acta* 422 (2) (2000) 187–198.
- [12] G.A. Eiceman, J. Gardea-Torresdey, F. Dorman, E. Overton, A. Bhushan, H.P. Dharmasena, Gas chromatography, *Anal. Chem.* 78 (12) (2006) 3985–3996.
- [13] H. Lin, M. Jang, K.S. Suslick, Preoxidation for colorimetric sensor array detection of VOCs, *J. Am. Chem. Soc.* 133 (42) (2011) 16786–16789.
- [14] C.-X. Yang, X.-P. Yan, Metal-organic framework MIL-101(Cr) for high-performance liquid chromatographic separation of substituted aromatics, *Anal. Chem.* 83 (18) (2011) 7144–7150.
- [15] F. Wang, Y. Yang, T.M. Swager, Molecular recognition for high selectivity in carbon nanotube/polythiophene chemiresistors, *Angew. Chem.-Int. Edit.* 47 (44) (2008) 8394–8396.
- [16] H.-J. Kim, J.-W. Yoon, K.-I. Choi, H.W. Jang, A. Umar, J.-H. Lee, Ultraselective and sensitive detection of xylene and toluene for monitoring indoor air pollution using Cr-doped NiO hierarchical nanostructures, *Nanoscale* 5 (15) (2013) 7066–7073.
- [17] H.-S. Woo, C.-H. Kwak, J.-H. Chung, J.-H. Lee, Co-doped branched ZnO nanowires for ultrasensitive and sensitive detection of xylene, *ACS Appl. Mater. Interfaces* 6 (24) (2014) 22553–22560.
- [18] S.C. Hernandez, C.M. Hangarter, A. Mulchandani, N.V. Myung, Selective recognition of xylene isomers using ZnO-SWNTs hybrid gas sensors, *Analyst* 137 (11) (2012) 2549–2552.
- [19] S. Li, J. Zheng, W. Zhang, J. Cao, S. Li, Z. Rao, Molecular recognition and quantitative analysis of xylene isomers utilizing cataluminescence sensor array, *Analyst* 138 (3) (2013) 916–920.
- [20] B. Wang, H. Tan-Phat, W. Wu, N. Hayek, D. Thu Trang, J.C. Cancilla, J.S. Torrecilla, M.M. Nahid, J.M. Colwell, O.M. Gazit, S.R. Puniredd, C.R. McNeill, P. Sonar, H. Haick, A highly sensitive diketopyrrolopyrrole-based ambipolar transistor for selective detection and discrimination of xylene isomers, *Adv. Mater.* 28 (21) (2016) 4012–4018.
- [21] J.M. Holcroft, K.J. Hartlieb, P.Z. Moghadam, J.G. Bell, G. Barin, D.P. Ferris, E.D. Bloch, M.M. Algaradah, M.S. Nassar, Y.Y. Botros, K.M. Thomas, J.R. Long, R.Q. Snurr, J.F. Stoddart, Carbohydrate-mediated purification of petrochemicals, *J. Am. Chem. Soc.* 137 (17) (2015) 5706–5719.
- [22] Y.-M. Zhang, N.-Y. Zhang, K. Xiao, Q. Yu, Y. Liu, Photo-controlled reversible microtubule assembly mediated by paclitaxel-modified cyclodextrin, *Angew. Chem.-Int. Edit.* 57 (28) (2018) 8649–8653.
- [23] L. Xiao, Y. Ling, A. Alsaibee, C. Li, D.E. Helbling, W.R. Dichtel, Beta-cyclodextrin polymer network sequesters perfluorooctanoic acid at environmentally relevant concentrations, *J. Am. Chem. Soc.* 139 (23) (2017) 7689–7692.
- [24] H. Huang, D. Xu, M. Liu, R. Jiang, L. Mao, Q. Huang, Q. Wan, Y. Wen, X. Zhang, Y. Wei, Direct encapsulation of AIE-active dye with beta cyclodextrin terminated polymers: Self-assembly and biological imaging, *Mater. Sci. Eng. C-Mater. Biol. Appl.* 78 (2017) 862–867.
- [25] Z. Aytac, S. Ipek, E. Durgun, T. Tekinay, T. Uyar, Antibacterial electrospun zein nanofibrous web encapsulating thymol/cyclodextrin-inclusion complex for food packaging, *Food Chem.* 233 (2017) 117–124.
- [26] S. Kubendhiran, R. Sakthivel, S.-M. Chen, B. Mutharani, T.-W. Chen, Innovative strategy based on a novel carbon-black-beta-cyclodextrin Nanocomposite for the Simultaneous determination of the anticancer drug flutamide and the environmental pollutant 4-nitrophenol, *Anal. Chem.* 90 (10) (2018) 6283–6291.
- [27] H. Bakirci, W.M. Nau, Chiral discrimination in the complexation of heptakis-(2,6-di-O-methyl)-beta-cyclodextrin with 2,3-diazabicyclo 2.2.2 oct-2-ene derivatives, *J. Photochem. Photobiol. a-Chem.* 173 (3) (2005) 340–348.
- [28] F. Chandra, S. Mallick, A.L. Koner, Spectroscopic investigation of bio-mimetic solvolysis of 6-(N, N-dimethylamino)-2,3-naphthalic anhydride in confined nanocavities, *PCCP* 19 (6) (2017) 4337–4344.
- [29] S. Mallick, A.S. Arathi, A.L. Koner, Customized tuning of aggregation-induced emission of a naphthalimide dye by surfactants and cyclodextrin, *J. Colloid Interface Sci.* 499 (2017) 46–53.
- [30] L. Jiang, J.W.J. de Folter, J. Huang, A.P. Philipse, W.K. Kegel, A.V. Petukhov, Helical colloidal sphere structures through thermo-reversible co-assembly with molecular microtubes, *Angew. Chem.-Int. Edit.* 52 (12) (2013) 3364–3368.
- [31] L. Jiang, Y. Yan, J. Huang, Zwitterionic surfactant/cyclodextrin hydrogel: microtubes and multiple responses, *Soft Matter* 7 (21) (2011) 10417–10423.
- [32] C. Zhou, X. Cheng, Q. Zhao, Y. Yan, J. Wang, J. Huang, Self-assembly of nonionic surfactant tween 20@2 beta-CD inclusion complexes in dilute solution, *Langmuir* 29 (43) (2013) 13175–13182.
- [33] Q. Zhao, Y. Wang, Y. Yan, J. Huang, Smart nanocarrier: self-assembly of bacteria-like vesicles with photoswitchable cilia, *ACS Nano* 8 (11) (2014) 11341–11349.
- [34] L. Jiang, Y. Peng, Y. Yan, J. Huang, Aqueous self-assembly of SDS@2 beta-CD complexes: lamellae and vesicles, *Soft Matter* 7 (5) (2011) 1726–1731.
- [35] L. Jiang, Y. Yan, M. Drechsler, J. Huang, Enzyme-triggered model self-assembly in surfactant-cyclodextrin systems, *Chem. Commun.* 48 (59) (2012) 7347–7349.
- [36] C. Zhou, J. Huang, Y. Yan, Chain length dependent alkane/beta-cyclodextrin nonamphiphilic supramolecular building blocks, *Soft Matter* 12 (5) (2016) 1579–1585.
- [37] X. Wang, M. Li, P. Song, X. Lv, Z. Liu, J. Huang, Y. Yan, Reversible manipulation of supramolecular chirality using host-guest dynamics between beta-cyclodextrin and alkyl amines, *Chem.-a Eur. J.* 24 (52) (2018) 13734–13739.
- [38] K.L. Yin, X. Qing, D.J. Xu, C.L. Chen, Constrain molecular dynamics simulation of 1: 1 inclusion of beta-cyclodextrin and p-cresol in nanodrip and vacuum systems, *Chin. J. Chem. Phys.* 17 (6) (2004) 711–716.
- [39] I. Sanemasa, Y. Akamine, Association Of benzene and alkylbenzenes with cyclodextrins in aqueous-medium, *Bull. Chem. Soc. Jpn.* 60 (6) (1987) 2059–2066.
- [40] R. Krishnan, A.M. Rakihi, K.R. Gopidas, Study of beta-cyclodextrin-pyromellitic diimide complexation. conformational analysis of binary and ternary complex structures by induced circular dichroism and 2D NMR spectroscopies, *J. Phys. Chem. C* 116 (47) (2012) 25004–25014.
- [41] H.J. Schneider, F. Hacket, V. Rudiger, H. Ikeda, NMR studies of cyclodextrins and cyclodextrin complexes, *Chem. Rev.* 98 (5) (1998) 1755–1785.
- [42] Y. Inoue, Y. Kanda, Y. Yamamoto, R. Chujo, S. Kobayashi, Elucidation of the host guest geometrical relationship in a branched cyclomaltohexaose inclusion-complex by measurement of the intermolecular nuclear overhauser effects in the rotating frame, *Carbohydr. Res.* 196 (1989) C8–C13.
- [43] M.V. Rekharsky, R.N. Goldberg, F.P. Schwarz, Y.B. Tewari, P.D. Ross, Y. Yamashoji, Y. Inoue, Thermodynamic and nuclear-magnetic-resonance study of the interactions of alpha-cyclodextrin and beta-cyclodextrin with model substances - phenethylamine, ephedrine, and related substances, *J. Am. Chem. Soc.* 117 (34) (1995) 8830–8840.
- [44] Y. Hou, S. Li, T. Sun, J. Yang, P. Xing, W. Liu, A. Hao, Organogels based on beta-cyclodextrin system with molecular recognition property, *J. Incl. Phenom. Macrocy. Chem.* 80 (3–4) (2014) 217–224.
- [45] M. Kajtar, C. Horvathotro, E. Kuthi, J. Szejtli, A simple rule for predicting circular-dichroism induced in aromatic guests by cyclodextrin hosts in inclusion complexes, *Acta Chim. Acad. Scientiarum Hungaricae* 110 (3) (1982) 327–355.
- [46] Y.A. Zhdanov, Y.E. Alekseev, E.V. Kompantseva, E.N. Vergeyichik, Induced optical-activity in cyclodextrin Complexes, *Usp. Khim.* 61 (6) (1992) 1025–1046.
- [47] S. Allenmark, Induced circular dichroism by chiral molecular interaction, *Chirality* 15 (5) (2003) 409–422.
- [48] A.J.M. Valente, O. Soderman, The formation of host-guest complexes between surfactants and cyclodextrins, *Adv. Colloid Interface Sci.* 205 (2014) 156–176.
- [49] L. Jiang, Y. Yan, J. Huang, Versatility of cyclodextrins in self-assembly systems of amphiphiles, *Adv. Colloid Interface Sci.* 169 (1) (2011) 13–25.
- [50] Y. He, X. Shen, Q. Chen, H. Gao, Characterization and mechanism study of micrometer-sized secondary assembly of beta-cyclodextrin, *PCCP* 13 (2) (2011) 447–452.
- [51] J. Wang, W. Qi, N. Lei, X. Chen, Lamellar hydrogel fabricated by host-guest interaction between alpha-cyclodextrin and amphiphilic phytoester ethoxylates, *Colloids Surf. a-Physicochem. Eng. Aspects* 570 (2019) 462–470.
- [52] S. Yang, Y. Yan, J. Huang, A.V. Petukhov, L.M.J. Kroon-Batenburg, M. Drechsler, C. Zhou, M. Tu, S. Granick, L. Jiang, Giant capsids from lattice self-assembly of cyclodextrin complexes, *Nature, Communications* 8 (2017).
- [53] L. Jiang, Y. Peng, Y. Yan, M. Deng, Y. Wang, J. Huang, “Annular Ring” microtubes formed by SDS@2 beta-CD complexes in aqueous solution, *Soft Matter* 6 (8) (2010) 1731–1736.
- [54] S. Ouhajji, J. Landman, S. Prevost, L. Jiang, A.P. Philipse, A.V. Petukhov, In situ observation of self-assembly of sugars and surfactants from nanometres to microns, *Soft Matter* 13 (13) (2017) 2421–2425.
- [55] B.M. Espinosa-Garcia, W.M. Arguelles-Monal, J. Hernandez, L. Felix-Valenzuela, N. Acosta, F.M. Goycoolea, Molecularly imprinted chitosan-genipin hydrogels with recognition capacity toward o-xylene, *Biomacromolecules* 8 (11) (2007) 3355–3364.
- [56] B. Barton, E.C. Hosten, P.L. Pohl, Discrimination between o-xylene, m-xylene, p-xylene and ethylbenzene by host compound (R, R)-(-)-2,3-dimethoxy-1,1,4,4-tetrahydropyridine-1,4-diol, *Tetrahedron* 72 (49) (2016) 8099–8105.